

Time-delay Cosmography: Increased Leverage with Angular Diameter Distances

I. Jee^a, E. Komatsu^{a,b}, S. H. Suyu^{c,a}, D. Huterer^{d,a,e}

^aMax-Planck-Institut für Astrophysik, Karl-Schwarzschild Str. 1, 85741 Garching, Germany

^bKavli Institute for the Physics and Mathematics of the Universe, Todai Institutes for Advanced Study, the University of Tokyo, Kashiwa, Japan 277-8583 (Kavli IPMU, WPI)

^cInstitute of Astronomy and Astrophysics, Academia Sinica, P.O. Box 23-141, Taipei 10617, Taiwan

^dDepartment of Physics, University of Michigan, 450 Church St, Ann Arbor, MI 48109-1040

^eExcellence Cluster Universe, Boltzmannstrasse 2, D-85748 Garching, Germany

E-mail: ijee@mpa-garching.mpg.de

Abstract. Strong lensing time-delay systems constrain cosmological parameters via the so-called time-delay distance and the angular diameter distance to the lens. In previous studies, only the former information was used in forecasting cosmographic constraints. In this paper, we show that the cosmological constraints improve significantly when the latter information is also included. Specifically, the angular diameter distance plays a crucial role in breaking the degeneracy between the curvature of the Universe and the time-varying equation of state of dark energy. Using a mock sample of 55 bright quadruple lens systems based on expectations for ongoing/future imaging surveys, we find that adding the angular diameter distance information to the time-delay distance information and the cosmic microwave background data of Planck improves the constraint on the constant equation of state by 30%, on the time variation in the equation of state by a factor of two, and on the Hubble constant in the flat Λ CDM model by a factor of two. Therefore, previous forecasts for the statistical power of time-delay systems were significantly underestimated, i.e., time-delay systems are more powerful than previously appreciated.

Contents

1	Introduction	1
2	Method	2
3	Single-probe constraints combined with the Planck distance prior	5
3.1	Time-delay lenses	5
3.2	BAO	9
3.3	SNe	9
3.4	Comparison to future BAO and SNe predictions	10
4	Pivot redshift	10
5	Conclusion	12
A	Lensing constraints on H_0	15
A.1	H_0 in ow CDM and ow_z CDM models	15
A.2	H_0 in flat Λ CDM model	16
B	Constraints assuming the flat universe	16

1 Introduction

The redshift-distance relation constrains cosmological parameters. The use of strong gravitational lens systems with time-delay measurements as a cosmological distance probe was suggested by Refsdal in 1964 [1], and has been extensively studied to measure the present value of the Hubble parameter, H_0 (see, e.g. [2]). The physical quantity of interest here is the so-called *time-delay distance* $D_{\Delta t}$. This is a distance-like quantity, given by a combination of three angular diameter distances in a strong lens system:

$$D_{\Delta t} \equiv (1 + z_L) \frac{D_A(EL)D_A(ES)}{D_A(LS)}, \quad (1.1)$$

where z_L is the redshift of the lens, while $D_A(EL)$, $D_A(ES)$ and $D_A(LS)$ are the angular diameter distances from the Earth to the lens, from the Earth to the source, and from the lens to the source, respectively. As each of the distance is proportional to the inverse of H_0 , $D_{\Delta t}$ is proportional to $1/H_0$. Ref. [3] has shown that a precise measurement of H_0 is important for constraining the equation-of-state parameter of dark energy, w . This motivated the measurement of time-delay distances in the recent years. However, the constraints weaken significantly when w is allowed to vary with time.

It is, in fact, possible to extract the angular diameter distance to the lens, $D_A(EL)$, by combining time-delay measurements with the lens stellar velocity dispersion measurements [4, 5]. The physics is simple: The time-delay measurement is the mass estimate of the lens galaxy, while the velocity dispersion measurement is the potential estimate. By knowing the mass and the potential, we can calculate the physical size of the system, thus the system can be used as the “ruler”. Comparing the observed separation of lensed images with the length

of the ruler, we can estimate $D_A(EL)$. In ref. [4], Paraficz and Hjorth demonstrated this for a singular isothermal sphere (SIS) lens without mass external to the lens along the line of sight. In ref. [5], we have extended the analysis by including the external convergence, allowing the mass profile of the lens to follow an arbitrary power-law, and allowing the velocity dispersion to be anisotropic. We have found that the main source of uncertainty for D_A is the unknown (anisotropic) velocity structure, which affects the normalization of the potential of the lens galaxy. We have also found that the mass external to the lens along the line of sight (external convergence) has no effect on the inferred $D_A(EL)$. In this paper, we show that the constraints on the cosmological parameters, especially on a time-varying w , improve significantly by including $D_A(EL)$.

The structure of the paper is as follows. In section 2, we introduce the mock catalog of the strong lens systems we use, and describe the cosmological model along with the fiducial cosmological parameters we use. In section 3, we compare the cosmological constraints we expect from lenses to those from the other cosmological distance probes, specifically, Type Ia Supernovae (SNe) and Baryon Acoustic Oscillation (BAO). In section 4 we introduce the pivot redshift and w_p - w_a parametrization, and show how lensing distances improve the figure of merit for the dark energy equation of state. We combine cosmological information from different probes to show the constraining power of strong lenses in practice, and conclude in section 5. In Appendix A, we show the constraint on the Hubble constant H_0 using the two lensing distances. In Appendix B, we show the dark energy constraints assuming that the universe is spatially flat.

2 Method

Each well-modeled time-delay lens system yields two distance(-like) quantities, $D_A(EL)$ and $D_{\Delta t}$. The uncertainties of $D_A(EL)$ and $D_{\Delta t}$ are dominated by the velocity dispersion and the external convergence, respectively. In this work we make an assumption that we can measure both distances with 5% uncertainty, which requires a few per cent measurement of the spatially resolved velocity dispersion of the lens galaxy, as well as a good understanding of the mass distribution along the line-of-sight, that is obtainable by simulations and observations of the lens environment [5, 6]. Regarding the lens mass model, the power-law density profile in ref. [5] is widely used due to its ability to fit the imaging data near the image positions. The local density profile is well reconstructed with the model if the images are spatially extended such that information from thousands of intensity pixels can be used. However, ref. [7, 8] have pointed out that the information obtained by the lensed images cannot uniquely determine the shape of lens mass profile due to the so-called *Source-Position Transformation* (SPT). Specifically, they focused on the degeneracy between composite density profiles and a power-law mass profile, and have shown that fixing the shape of the lens mass profile as a power law can break the SPT. However, they have also mentioned that these models can be distinguished if more information is available: for example, if more than three images with time delays are observed, the degeneracy can be broken as the general SPT does not conserve the time delay ratios. In ref. [6], the robustness of the measured time-delay distance is tested with power law and composite model under the presence of lens kinematics data and shown to be nearly independent of the choice of the model. Ref. [9] has shown that the so-called *Mass-Sheet Transformation* (MST), which is a special case of the SPT, scales the time delays by the same factor, and thus conserves the time-delay ratio, can bias the mass modeling. However, ref. [10] has empirically shown using the Illustris simulation that most

of the early-type galaxies with high ($\sigma > 200\text{kms}^{-1}$) velocity dispersion, which most of the lens galaxies are, show nearly power-law behavior. The MST degeneracy can also be broken if additional information on the lens galaxy (e.g. velocity dispersion) is obtained. Ref. [11] has shown that the existence of substructures in the lens galaxy perturbs the time delay: However, the effect of perturbation on the time delays (<1 day) is typically smaller than the currently available time-delay measurement uncertainties, and thus both distances are mainly determined by the global mass distribution rather than the substructures. Thus we claim that this precision measurements on both distances is possible, but only when good quality imaging / kinematics data as well as time-delay measurements are available. The correlation between the two distances is negligible, because the uncertainties in the velocity dispersion and the external convergence are uncorrelated.

To study the expected cosmological constraints from lenses, we need to specify the distribution of lens and source redshifts. We use the catalog of mock lenses in ref. [12] to obtain the redshift distribution of time-delay lenses with double and quadruple images expected for the Large Synoptic Survey Telescope (LSST) [13, 14]. Although LSST itself is expected to find around ten thousand lensed quasars, there are only about 400 systems that would have good time delay measurements [15]. To obtain distances from a lens system with a reasonable accuracy, a good mass model of the lens galaxy is also required, as both the time-delay distance and the angular diameter distance are sensitive to the mass distribution of the lens. Ancillary data both in terms of high-resolution imaging and spectroscopy of the lens systems are needed for accurate lens mass modeling. Therefore, we select lens systems from the mock catalog with the following criteria for acquiring ancillary data with relative ease: (1) the quasar image separation is $> 1''$, (2) the third brightest quasar image has an i -band magnitude $m_i < 21$, and (3) the lens galaxy has $m_i < 22$. The criteria on the quasar image separation and brightness make it easier to measure the time delays with high precision (uncertainty of a few percent). Furthermore, a sufficiently wide quasar image separation is required for extracting the Einstein ring of the quasar host galaxy and measuring the lens velocity dispersion for mass modeling. The lens galaxy also needs to be of sufficient brightness for measuring the lens velocity dispersion. In this work, we focus on quadruply imaged lens systems as they provide more information than doubly imaged systems. After applying these criteria to the LSST mock lens sample, we obtain 55 quadruple lens systems as the best cases of obtaining ancillary data.

Figure 1 shows the source and the lens redshift distribution of quadruple lenses in our mock catalog. For the visualization purpose, only in this figure, the total number of detectable lenses is oversampled by a factor of 5 (based on the catalog from ref. [12]) to populate the histogram. The expected constraints reported in this paper are derived from the actual distribution of the 55 lenses.

Since these are the bright lens systems, a fraction of these systems will already be discovered in the current imaging surveys. In particular, we expect that $\sim 25\%$ of these systems will be discovered in the Dark Energy Survey (DES)¹ and the Hyper Suprime-Cam (HSC; [16])² Survey. Furthermore, we expect a few more quadruple lens systems from the northern areas of the HSC Survey that are not covered in DES and LSST. Therefore, even though we focus here on the LSST sample, our cosmographic predictions are also relevant for the upcoming years before the LSST era as new lens systems in the current imaging surveys are discovered and monitored.

¹<http://www.darkenergysurvey.org/index.shtml>

²<http://www.naoj.org/Projects/HSC/surveyplan.html>

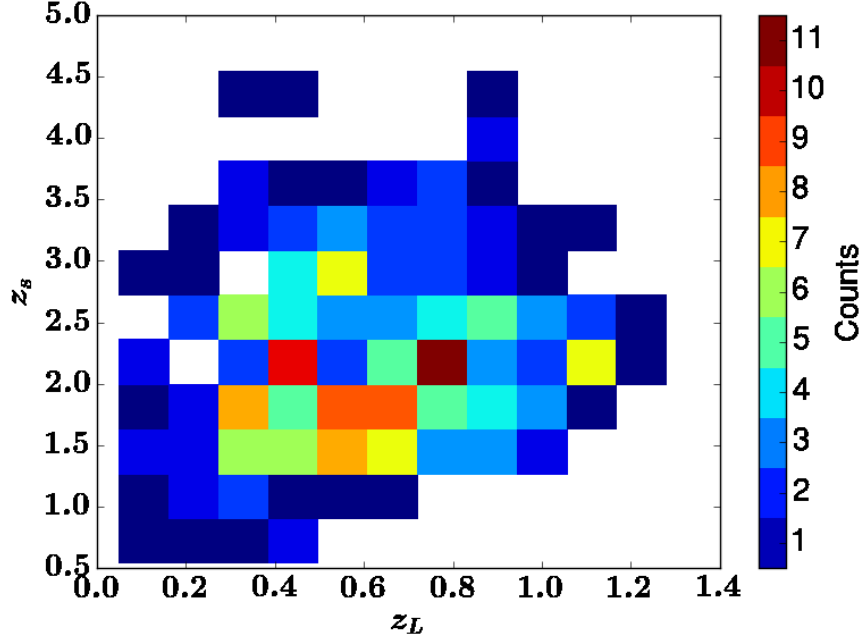


Figure 1: The distribution of source (z_S) and lens (z_L) redshifts of quadruply imaged time-delay lenses expected for LSST [12]. These lens systems are the best ones to obtain ancillary data and measure distances with 5% precision. For visualization purposes, the number of the lenses is oversampled by a factor of five only in this figure (thus each pixel does not necessarily have a multiple-of-5 value).

We explore constraints on two variations of Λ CDM model. Both assume a curved universe ($\Omega_k \neq 0$) and an unknown equation of state of dark energy ($w \neq -1$). The first model assumes that w is a constant (owCDM) with the following cosmological parameters:

$$\vec{\theta} \in \{\Omega_m, \Omega_k, w, h\} \quad (\text{owCDM model}). \quad (2.1)$$

The second model further assumes that w varies in time with $w = w_0 + (1 - a)w_a$ [17] (ow_zCDM):

$$\vec{\theta} \in \{\Omega_m, \Omega_k, w_0, w_a, h\} \quad (\text{ow}_z\text{CDM model}). \quad (2.2)$$

We choose the fiducial cosmology following Planck 2015 ($\Omega_m = 0.308$, $\Omega_k = 0$, $w_0 = -1$, $w_a = 0$, and $h = 0.678$) [18].

We use the Fisher information matrix (hereafter the Fisher matrix) to calculate the constraining power of the cosmological probes. For a data vector $\vec{d}(\vec{\theta})$ with a set of parameters $\vec{\theta}$, the Fisher matrix \mathbf{F} is given by

$$F_{ij} = \sum_{\alpha\beta} \frac{\partial d_\alpha}{\partial \theta_i} \mathbf{Cov}_{\alpha\beta}^{-1} \frac{\partial d_\beta}{\partial \theta_j}, \quad (2.3)$$

where indices α and β run over the observables, and $\mathbf{Cov}(\vec{d})$ is the data covariance matrix. For lenses, $\mathbf{Cov}_{\alpha\beta} = \delta_{\alpha\beta} \sigma_\alpha^{-2}$, where $\delta_{\alpha\beta}$ is the Kronecker delta as we assume no correlation between the different lens systems and between the two measured lensing distances D_A

and $D_{\Delta t}$ of each lens system. The uncertainty in each distance σ_α is $\sigma_\alpha = 0.05d_\alpha$ as we assume 5% precision measurements of both distances. The inverse of the Fisher matrix, \mathbf{F}^{-1} , gives the covariance matrix of the parameters, and the marginalized uncertainty on the i -th parameter is calculated as $(\mathbf{F}^{-1})_{ii}^{1/2}$. If the normalization of \mathbf{F} increases by a factor of n , then the normalization of the parameter covariance matrix decreases by a factor of n , thus the error bar on each parameter tightens by a factor of \sqrt{n} .

3 Single-probe constraints combined with the Planck distance prior

In this section we investigate the constraining power of the time-delay lenses expected from LSST in section 3.1, and compare the constraints to that of two other cosmological distance probes, the BAO data from Baryon Oscillation Spectroscopic Survey (BOSS) data release (DR) 11 in section 3.2, and the SNe data from Joint Light-curve Analysis (JLA) in section 3.3. We examine the future prospects of constraints from BAO and SNe using LSST data in section 3.4. We combine each probe with the CMB distance prior calculated from the Planck 2015 result [19]. The distance prior is calculated using the shift parameter, R_{shift} , and the multipole corresponding to the sound horizon at the moment of last scattering, l_* . The definitions of these parameters are

$$\begin{aligned} R_{\text{shift}} &\equiv \sqrt{\Omega_m H_0^2 D_A(z_*)}/c, \\ l_* &\equiv \pi \frac{D_A(z_*)}{r_s(z_*)}, \end{aligned} \tag{3.1}$$

where $z_* = 1089.94$ is the redshift of the last scattering surface, and $r_s(z_*) = 144.89$ Mpc is the size of the sound horizon at redshift z_* . The distance prior compresses information in the CMB power spectrum relevant for dark energy to two numbers.

3.1 Time-delay lenses

We first show how sensitive $D_{\Delta t}$ and $D_A(EL)$ are to w_0 and w_a as a function of z_L and z_S .

In figure 2, we show $\partial \ln T / \partial p$ (where $T = (D_A, D_{\Delta t})$ and $p = (w_0, w_a)$). The larger the absolute value of $\partial \ln T / \partial p$ is, the bigger the unmarginalized sensitivity of the distance T becomes to the parameter p , with all the other cosmological parameters fixed at the fiducial values. Also, equation 2.3 shows that the information is proportional to $\partial T / \partial p$. The higher z_L is, the more sensitive $D_{\Delta t}$ becomes to both w_0 and w_a for a given z_S , and vice versa. We find that D_A is always more sensitive to w_a , when all the other parameters are fixed at the fiducial values.

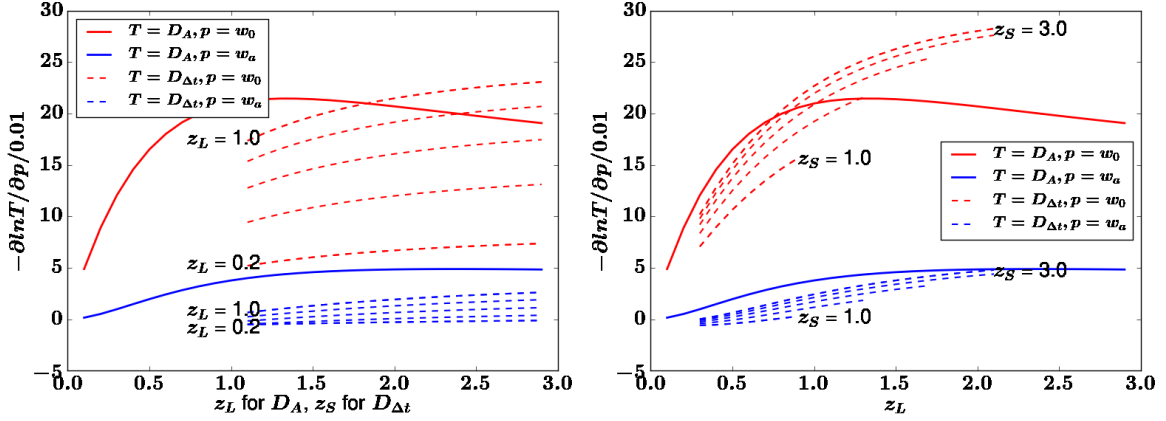


Figure 2: Logarithmic derivatives of distances $T = (D_A, D_{\Delta t})$ with respect to the cosmological parameters $p = (w_0, w_a)$, as a function of redshift. Left panel: The solid lines show $T = D_A$, while the dashed lines show $T = D_{\Delta t}$, with various combinations of the lens and the source redshift. Each dashed line corresponds to one z_L in range $[0.2, 1.0]$ in increments of 0.2, and shows $-\partial \ln D_{\Delta t} / \partial p / 0.01$ as a function of z_S . We only show z_S which is higher than the highest z_L in this range. Right panel: The solid lines show $-\partial \ln D_A / \partial p / 0.01$ as a function of z_L . Each dashed line corresponds to one z_S in range $[1.0, 3.0]$ in increments of 0.5, and shows $-\partial \ln D_{\Delta t} / \partial p / 0.01$ as a function of z_L . We only show z_L which is lower than the lowest z_S in this range. Both panels show that D_A is always more informative than $D_{\Delta t}$ for constraining w_a (i.e., $|\partial \ln D_A / \partial w_a| > |\partial \ln D_{\Delta t} / \partial w_a|$), and D_A is often more informative than $D_{\Delta t}$ on w_0 .

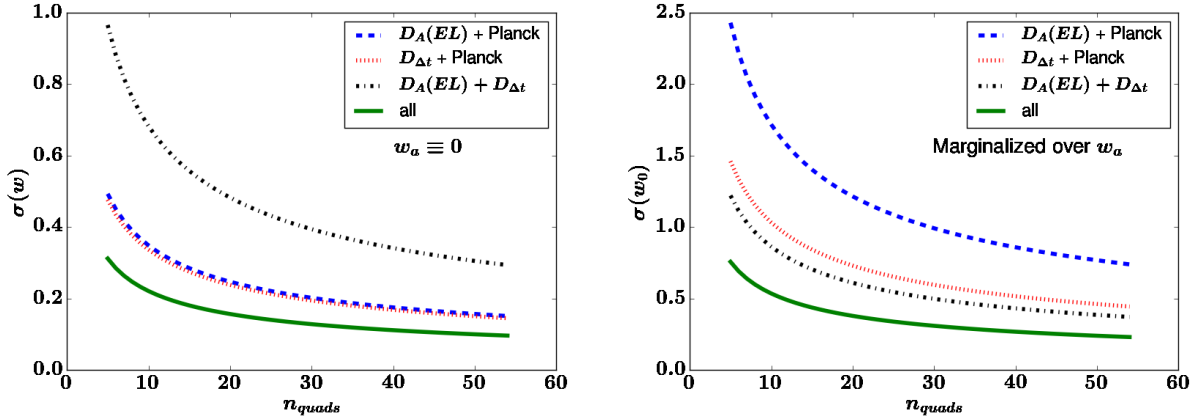


Figure 3: The $1\text{-}\sigma$ uncertainty in w , denoted as $\sigma(w)$, and that in w_0 , denoted as $\sigma(w_0)$, from time-delay lenses as a function of the number of lenses for the left and the right panel, respectively. The black dash-dot line is the lens-only data, while the other lines use the Planck distance priors combined with D_A (blue dashed), $D_{\Delta t}$ (red dotted), or both (green) from lenses. (Left) $ow\text{CDM}$ model. (Right) $ow_z\text{CDM}$ model marginalized over w_a , as well as all the other parameters.

In figure 3, we show the expected $1\text{-}\sigma$ uncertainties in w for the $ow\text{CDM}$ model and w_0 for the $ow_z\text{CDM}$ model (combined with the Planck distance priors), with all the other pa-

rameters marginalized over. As the Fisher matrix is proportional to n_{quads} , the marginalized uncertainty in $D_A(EL) + D_{\Delta t}$ scales as $\propto 1/\sqrt{n_{\text{quads}}}$. For ow CDM (left panel of figure 3), the Planck distance priors combined with either D_A (blue dashed line) or $D_{\Delta t}$ (red dotted) from lenses improve the constraint on w significantly compared to the lens-only case (black dash-dot). Combining all improves the constraint further by 30%, in comparison to that of the $D_{\Delta t} + \text{Planck}$. For ow_z CDM (right panel of figure 3), we find that the lens-only ($D_A + D_{\Delta t}$) breaks the degeneracy between w_0 and the other parameters more efficiently than either combination of Planck + D_A or Planck + $D_{\Delta t}$, yielding a tighter constraint. Combining all improves the constraint further by a factor of 2 in comparison to $D_{\Delta t} + \text{Planck}$.

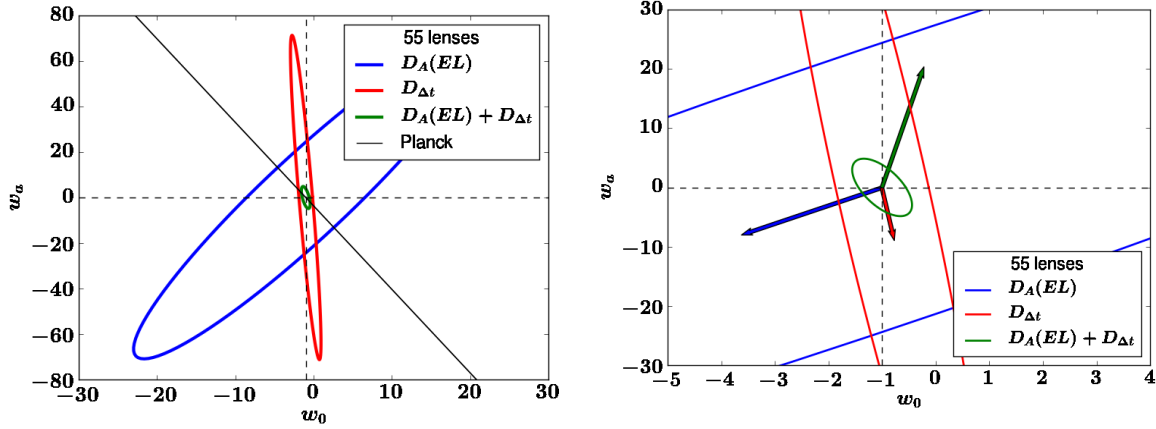


Figure 4: (Left) The 68 per cent CL in the w_0 - w_a plane constrained from 55 lenses for the ow_z CDM model. The blue line is the marginalized constraint from D_A , the red line is the marginalized constraint from $D_{\Delta t}$, and the green line is the marginalized constraint from the combination of the D_A and $D_{\Delta t}$. The black line is the unmarginalized constraint from Planck only. The horizontal and vertical dashed lines correspond to the fiducial values of $w_0 = -1$ and $w_a = 0$, respectively. (Right) Zoom in of the left panel, with degeneracy directions plotted as arrows. The arrows show the response of w_0 and w_a to the shift $\Delta\Omega_k = 0.02$. The blue arrow is the response for $D_A(EL)$, the red arrow is for $D_{\Delta t}$, and the green arrow is for the combination of two. The larger the arrow is relative to the contour, the more sensitive the distance is to Ω_k . The alignment between the arrows and the major axis of the contours indicate that the constraints from D_A (the red arrow and the red contour) and $D_{\Delta t}$ (the blue arrow and the blue contour) are individually dominated by Ω_k . However, the degeneracy between Ω_k and w is shown to be broken when D_A and $D_{\Delta t}$ are combined. For visualization purposes, the sizes of the arrows are inflated by a factor of 100.

The left panel of figure 4 is useful for understanding these results. The marginalized uncertainties in w_a from either D_A or $D_{\Delta t}$ individually are similar. The Planck distance prior (the black line) provides a degenerate combination of w_0 and w_a , thus cannot be marginalized. However, it is nicely orthogonal to the ones from D_A (the blue contour) and $D_{\Delta t}$ (the red contour). Thus, including the combination of D_A and Planck with the previous lensing constraints from $D_{\Delta t}$ reduces the uncertainty in w_a significantly. We also note that the constraint on w_a from $D_A + D_{\Delta t}$ (the green contour) is significantly tighter than the naive addition of the blue and the red contour, which indicates that this combination of distances effectively breaks the degeneracy between the equation of state of dark energy and the other

parameters over which we marginalize.

Next, we study the degeneracy structure of parameters constrained from lensing distances, by shifting a parameter and calculating the response of the other parameters to the shift in order for the likelihood to be maximized. Specifically, we describe the degeneracy between the curvature density Ω_k and the equation of state parameters w_0 and w_a . When Ω_k is shifted by an amount $\Delta\Omega_k$, to maximize the likelihood at the new fiducial value $\Omega_k + \Delta\Omega_k$, all the other parameters have to be shifted accordingly. The general expression for the shift in an arbitrary parameter $\Delta\theta_i$ due to a shift in a fixed, single parameter $\Delta\theta_k$ that maximizes the likelihood can be calculated as

$$\Delta\theta_i = \Delta\theta_k \frac{(\mathbf{F}^{-1})_{ik}}{(\mathbf{F}^{-1})_{kk}}, \quad (3.2)$$

where \mathbf{F}^{-1} is the inverse of the Fisher matrix. In figure 4, the right panel shows the projection of the shift vectors to w_0 - w_a plane as arrows, along with the marginalized constraint contour at the fiducial parameter to display it quantitatively. For each of D_A and $D_{\Delta t}$, the degeneracy directions are parallel to the major axes of the contours, which indicates that the degeneracies with Ω_k dominate the dependences of w_0 and w_a to other parameters. However, when the two distances are combined, the curvature degeneracy breaks and the alignment between the error contour and the shift disappears (the green arrow and the green contour are not aligned). The relative size of the arrow to the contour shows the sensitivity of the probe to Ω_k : the bigger the vector is with respect to the contour, the more sensitive the probe is to the change in Ω_k . By comparing the relative size of the red and the blue arrows to the red and the blue contours, we show that D_A and $D_{\Delta t}$ are comparably sensitive to $\Delta\Omega_k$, but the combination of two increases the sensitivity significantly (the green arrow and the green contour).

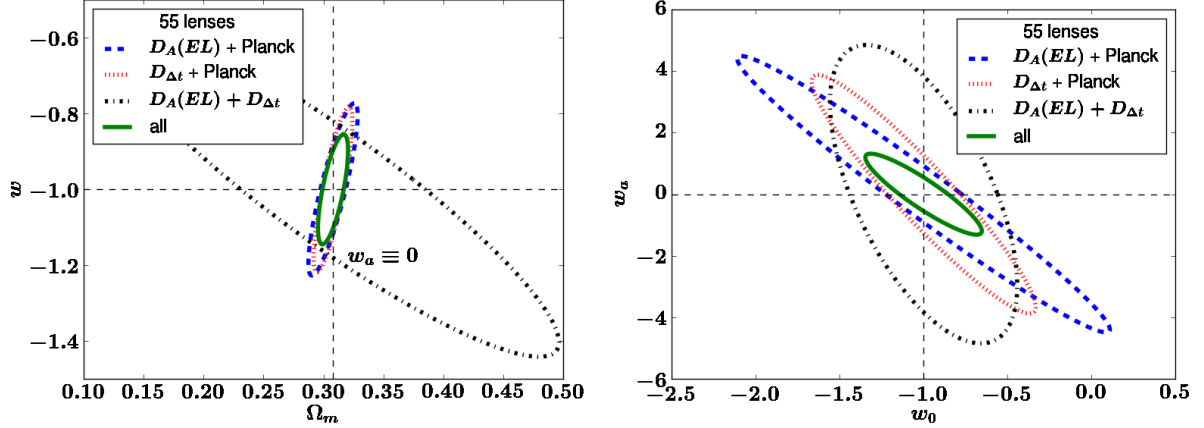


Figure 5: The marginalized 68 per cent CL constraints from 55 lenses in the (left) Ω_m - w plane for the ow CDM model, and (right) w_0 - w_a plane for the ow_z CDM model. The black dash-dot lines show the lens-only constraints from $D_A + D_{\Delta t}$, the blue dashed lines the constraints from $D_A + \text{Planck}$, the red dotted lines the constraints from $D_{\Delta t} + \text{Planck}$, and the green solid lines the combination of the two distances + Planck.

The left panel of figure 5 shows the joint constraints on Ω_m and w for ow CDM. We find that the Planck distance prior plays an important role in constraining Ω_m , while using both

D_A and $D_{\Delta t}$ combined with Planck distance prior improves the constraint on w by about 30% compared to the case of $D_{\Delta t}$ combined with Planck distance prior. The right panel of figure 5 shows the same for w_0 and w_a for ow_z CDM. We also show the lensing distances + Planck constraint on H_0 in Appendix A.

Next, we compare these constraints with those from Planck + BAO and Planck + SNe. We calculate the constraints from BAO and SNe using currently available data (BOSS DR11 for BAO, JLA sample for SNe).

3.2 BAO

BOSS DR11 provides the volume-averaged distance, $D_V \equiv (cz(1+z)^2 D_A^2/H)^{1/3}$, at two effective redshifts (0.32, 0.57) obtained from the BAO peak position in the spherically averaged two-point functions. The lower redshift is the LOWZ sample, and the higher redshift is the CMASS sample. Also, by separately measuring the two point functions along the line of sight and the direction perpendicular to it, the DR11 CMASS sample separately constrains the angular diameter distance D_A and the Hubble parameter H at $z = 0.57$ [20, 21]. To account for the correlation among D_V , D_A and H , we use the full likelihood of the CMASS sample for the analysis provided by the BOSS collaboration [20].

In our analysis we assume that the sound horizon scale at the baryon drag epoch, $r_{s,drag}$, is fixed as $r_{s,drag} = 149.28$ Mpc [20]. We then combine the cosmological constraints from D_V at $z = 0.32$, and D_A and H at $z = 0.57$ with the Planck distance prior. We calculate the Fisher matrix by taking the derivatives of the log likelihood at the fiducial cosmology. The results are shown in figure 6. The precision of the BAO data yields the narrowest contours on the Ω_m - w (for ow CDM) and w_0 - w_a (for ow_z CDM) planes. However, due to the limited number of redshifts ($z = 0.35$ and $z = 0.57$), the degeneracy is not broken efficiently; thus, the expected Planck + lens from 55 lenses can improve the constraints significantly, even though the precision of lensing data per redshift is not as precise as BAO.

3.3 SNe

We now study the constraints from Planck + SNe. We use the JLA data [22] to calculate the constraints from SNe. JLA uses Supernovae Legacy Survey (SNLS), Sloan Digital Sky Survey-II (SDSS-II) Supernova survey and a few low-redshift samples. The redshift of subsamples are: the low-redshift sample ($z < 0.1$), SDSS-II ($0.05 < z < 0.4$), and SNLS ($0.2 < z < 1$). There are 740 spectroscopically confirmed type Ia SNe in JLA. SDSS-II is used for anchoring the distances, and also an empirical relation between the host galaxies and the supernovae brightness is used as an extra calibration for the absolute magnitude of the SNe. For the calibration, there are 4 additional nuisance parameters that are taken into account in JLA: α , which scales the stretch of the light curve in time-domain; β , which scales the color at the peak of the light curve; M , which is the absolute B band magnitude of the SNe at the peak of the light curve; and Δ_M , which characterizes the peak absolute magnitude change due the stellar mass of the host galaxy.

We use Montepython [23] to sample the JLA likelihood. Specifically, we run Markov Chain Monte Carlo to sample the likelihood surface, and compute the covariance matrix in the cosmological parameters. We then use its inverse as the JLA Fisher matrix. The results are shown in figure 6. While the absolute distances, such as those from BAO and lenses, are effective at measuring Ω_k when combined with CMB [24], the relative distances from SNe are not. Thus, when Ω_k is set free, the constraints on Ω_m for ow CDM from 55 lenses combined with Planck are significantly better than those from 740 SNe combined with Planck.

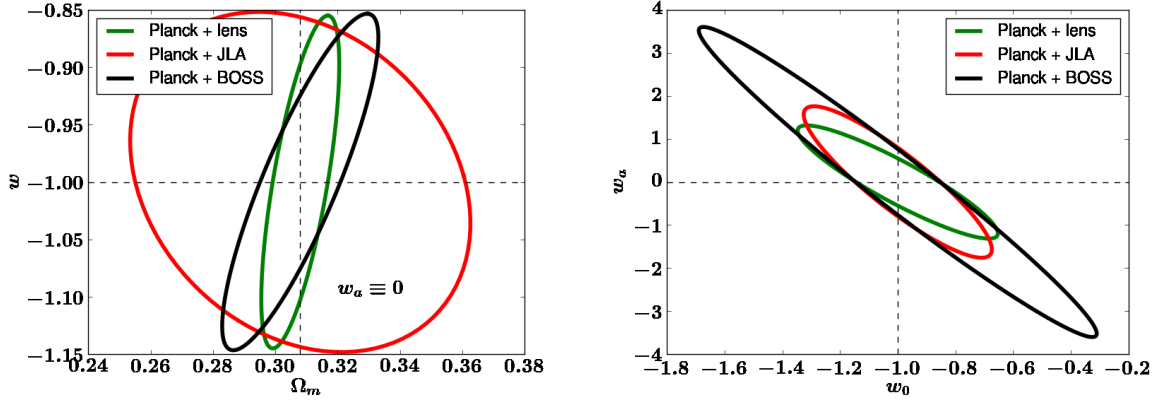


Figure 6: The marginalized 68 per cent CL constraints from strong lenses, SNe, and BAO, each combined with the Planck distance prior, in the (left) Ω_m - w_a plane for the ow_{CDM} model, and (right) w_0 - w_a for the $ow_z\text{CDM}$ model. The green lines show the constraints from Planck + lens, the red lines Planck + JLA, and the black lines Planck + BOSS.

3.4 Comparison to future BAO and SNe predictions

With several billion galaxies expected to be detected with LSST, BAO will allow measurements of distances with $\sim 2\%$ precision in the redshift range $1 < z < 3$ [25]. Combined with Planck, BAO will constrain w_0 with uncertainty ~ 0.4 and w_a with ~ 1 [26]. Also, 500,000 SNe are expected to be detected in 10 years of LSST operation in the redshift range $0.1 < z < 1.2$. With a subsample of 50,000 SNe only, the data will constrain w_0 with uncertainty ~ 0.05 , and w_a to order unity, assuming a flat universe [13]; in combination with Planck, the full sample of SNe constraints will be ~ 0.25 for w_0 and ~ 1.2 for w_a for the $ow_z\text{CDM}$ model [26]. We note that a modest sample of 55 lenses combined with the Planck distance prior constrains w_0 and w_a to ~ 0.4 and ~ 1.2 , respectively (see, e.g., Figure 6), which is comparable in precision to those expected from future BAO or SNe samples in the LSST era, when each is combined with Planck. Therefore, strong lenses provide an independent and competitive probe of dark energy. Needless to say, lensing, SNe, and BAO are affected by different systematic errors, and thus cross-checking the results using these three low-redshift probes of the expansion of the universe will be powerful.

4 Pivot redshift

The equation of state of dark energy, $w(z)$, can be re-written as

$$w = w_0 + (1 - a)w_a = w_p + (a_p - a)w_a, \quad (4.1)$$

where $w_p \equiv w_0 + (1 - a_p)w_a$ [27]. In this parameterization, the *pivot redshift* $z_p = \frac{1}{a_p} - 1$ is defined as the redshift where the uncertainty in w is minimized. The uncertainty in w_p shows how well a probe can measure the equation of state w , as w_p is orthogonal to w_a by construction, and thus is not coupled to the time variation of w [27, 28]. z_p shows at which redshift the main constraint on w is coming from: this pivot redshift varies depending on the probes, their redshift distributions and the measurement uncertainties, and can be negative.

Cosmological model	Probe	z_p	$\sigma(w_p)$	$\sigma(w_a)$	FoM
Flat, fixed Ω_m	CMB+BAO+SNe	0.288	0.0375	0.364	73.3
	Lens+CMB+BAO+SNe	0.487	0.0296	0.166	204
Flat, marginalized over Ω_m	CMB+BAO+SNe	0.358	0.0487	0.413	49.7
	Lens+CMB+BAO+SNe	0.386	0.0310	0.363	88.9
Marginalized over Ω_m and Ω_k (ow_z CDM)	CMB+BAO+SNe	0.215	0.0625	1.03	15.5
	Lens+CMB+BAO+SNe	0.245	0.0479	0.621	33.6

Table 1: Pivot redshift, z_p , uncertainties in w_p and w_a , and the Figure of Merit (FoM) for Planck + BOSS + JLA and Lens + Planck + BOSS + JLA. We test three cases: (1) $\Omega_k = 0$ and $\Omega_m = 0.309$, (2) $\Omega_k = 0$ and marginalized over Ω_m , and (3) marginalized over both Ω_k and Ω_m . As there is no correlation between w_p and w_a , $\text{FoM} = 1/(\sigma(w_p)\sigma(w_a))$.

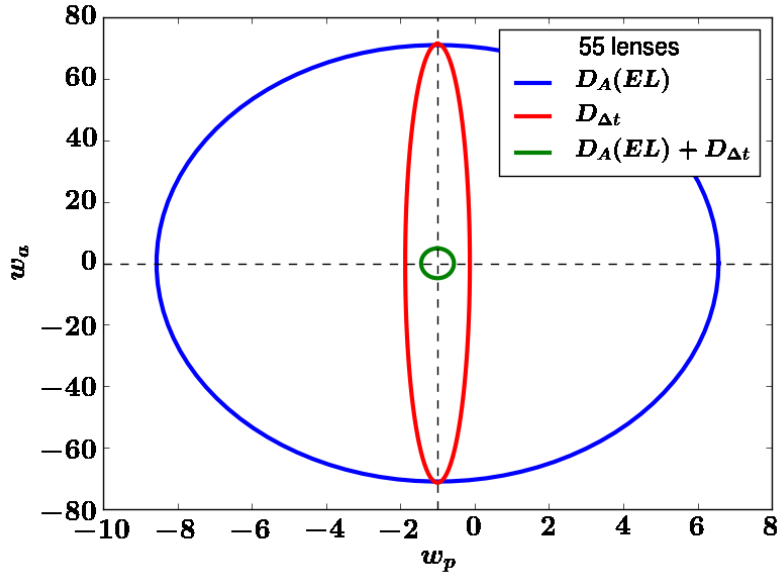


Figure 7: Same as figure 4, but in w_p - w_a plane. z_p is calculated separately for each probe: $z_p(D_A) = -0.226$, $z_p(D_{\Delta t}) = 0.0251$, and $z_p(D_A + D_{\Delta t}) = 0.0759$.

Figure 7 shows the constraints on (w_p, w_a) using the lens distances alone in w_p - w_a plane. The constraint on w_p from D_A alone is much weaker than that from $D_{\Delta t}$, while the constraints on w_a from both distances are comparable. However, by combining the two distance measures, the constraint on w_p improves by a factor of 2, and that on w_a improves by a factor of 24, due to complementary degeneracy directions as shown in figure 4.

The pivot redshift, z_p , and the uncertainties in w_p and w_a for two combinations of probes (Planck + BOSS + JLA, and 55 lenses (denoted by Lens) + Planck + BOSS + JLA) for three different cosmological cases ((1) $\Omega_k = 0$ and $\Omega_m = 0.309$, (2) $\Omega_k = 0$ and marginalized over Ω_m , and (3) marginalized over both Ω_k and Ω_m) are summarized in table 1. In comparison to Planck + BOSS + JLA, adding 55 lenses tightens the FoM by a factor of 2.78, 1.62 and 2.32 for the three models, respectively. In particular, when Ω_k is allowed to

vary, the uncertainty in w_a is reduced by almost a factor of 2 by including the lenses, which shows that the combination of D_A and $D_{\Delta t}$ is powerful in breaking the Ω_k - w degeneracy. This is consistent with our argument in section 3.1. Also z_p becomes higher as we include the lens distances in every case, which is typically beneficial when combining these probes of geometry with probes of the growth of cosmic structure.

5 Conclusion

There is more valuable cosmological information in the strongly lensed systems than measurements of the Hubble constant from time delays. In this paper, we have demonstrated that the addition of the angular diameter distance measurements to the quantity ($D_{\Delta t}$) that captures the cosmological information from time delays in the same sample of lenses provides crucial help in breaking cosmological parameter degeneracies. This improvement is most significant in some of the most interesting parameterizations that are currently being studied, such as when curvature of the universe and the time-variation in the equation of state of dark energy are allowed to be nonzero.

We have calculated the lensing constraints based on the predictions for the LSST survey, adopting a catalog of 55 quadruply imaged lenses (out of a much larger total number) that should have sufficiently good information that all observable quantities of interest in the lenses can be accurately measured. We have combined the forecasted lensing information from both the angular diameter distance and the time-delay distance. We then compared this lensing constraints with that from the BOSS DR11 and from the JLA type Ia supernova sample – each combined with the Planck 2015 distance prior.

We find that the combined lensing information significantly helps constrain the cosmological parameters, particularly when curvature is allowed to vary and when the equation of state of dark energy is allowed to be time-dependent. For example, lensing information would improve the current BAO+CMB+SN constraints on w_a by a factor of two, and those on the overall figure of merit of dark energy by about a factor of two relative to the case with no lensing (see Table 1 and figure 8). Key to this significant improvement is lensing’s ability to break the degeneracy between curvature and the equation of state parameters; see figure 4.

We are therefore very optimistic about the prospects of a select, accurately observed subsample of strong gravitational lenses to improve our constraints on dark energy. Fortunately, the lensing samples are a guaranteed product of the current and upcoming wide-field, deep surveys such as HSC, DES and LSST.

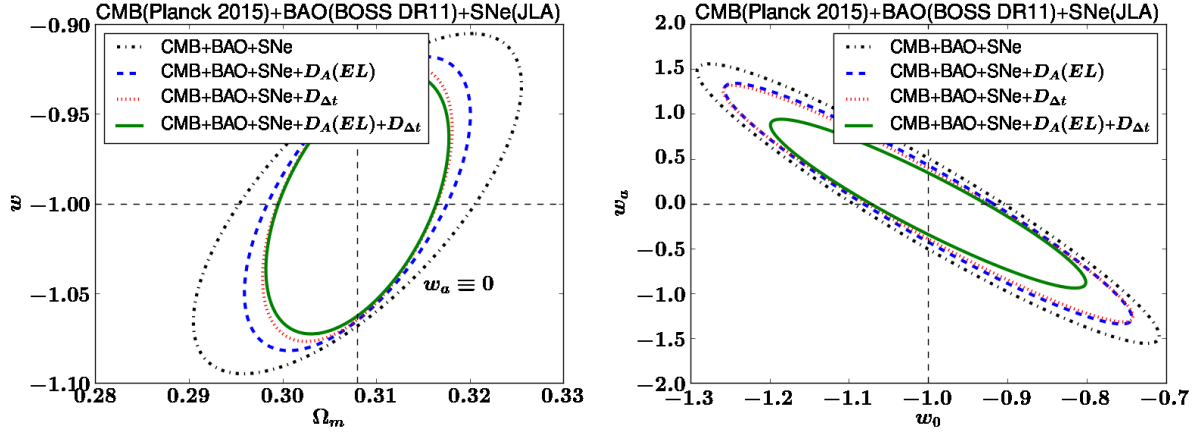


Figure 8: The marginalized 68 per cent CL from strong lenses, combined with Planck, BAO and SNe in the (left) Ω_m - w plane for the ow CDM model, (right) w_0 - w_a for the ow_z CDM model.

Acknowledgments

We thank Stefan Hilbert, Phil Marshall, Jan Grieb, and Ariel Sánchez for providing helpful information on the analysis. We thank Eric Linder for helpful comments, which helped identify an error in our Fisher matrix calculation for Ω_m and Ω_k in the first draft of the paper. We also thank Peter Schneider and Phil Marshall for the comments and the discussions for the paper. DH has been supported by NSF under contract AST-0807564 and DOE under contract DE-FG02-95ER40899, and also by the DFG cluster of excellence “Origin and Structure of the Universe” (www.universe-cluster.de).

References

- [1] S. Refsdal, *On the possibility of determining Hubble’s parameter and the masses of galaxies from the gravitational lens effect*, *Mon.Not.Roy.Astron.Soc.* **128** (1964) 307.
- [2] S. Suyu, P. Marshall, M. Auger, S. Hilbert, R. Blandford, et al., *Dissecting the Gravitational Lens B1608+656. II. Precision Measurements of the Hubble Constant, Spatial Curvature, and the Dark Energy Equation of State*, *Astrophys.J.* **711** (2010) 201–221, [[arXiv:0910.2773](https://arxiv.org/abs/0910.2773)].
- [3] W. Hu, *Dark energy probes in light of the CMB*, *ASP Conf.Ser.* **339** (2005) 215, [[astro-ph/0407158](https://arxiv.org/abs/astro-ph/0407158)].
- [4] D. Paraficz and J. Hjorth, *Gravitational lenses as cosmic rulers: Ω_m , Ω_Λ from time delays and velocity dispersions*, *Astron. Astrophys.* **507** (2009) L49–L52, [[arXiv:0910.5823](https://arxiv.org/abs/0910.5823)].
- [5] I. Jee, E. Komatsu, and S. H. Suyu, *Measuring angular diameter distances of strong gravitational lenses*, [arXiv:1410.7770](https://arxiv.org/abs/1410.7770).
- [6] S. Suyu, T. Treu, S. Hilbert, A. Sonnenfeld, M. Auger, et al., *Cosmology from gravitational lens time delays and Planck data*, *Astrophys.J.* **788** (2014) L35, [[arXiv:1306.4732](https://arxiv.org/abs/1306.4732)].
- [7] P. Schneider and D. Sluse, *Mass-sheet degeneracy, power-law models and external convergence: Impact on the determination of the Hubble constant from gravitational lensing*, *Astron. Astrophys.* **559** (2013) A37, [[arXiv:1306.0901](https://arxiv.org/abs/1306.0901)].
- [8] P. Schneider and D. Sluse, *Source-position transformation – an approximate invariance in strong gravitational lensing*, *Astron. Astrophys.* **564** (2014) A103, [[arXiv:1306.4675](https://arxiv.org/abs/1306.4675)].

- [9] E. E. Falco, M. V. Gorenstein, and I. I. Shapiro, *On model-dependent bounds on $H(0)$ from gravitational images Application of Q0957 + 561A,B*, *Astrophys.J* **289** (1985) L1–L4.
- [10] D. Xu, D. Sluse, P. Schneider, V. Springel, M. Vogelsberger, D. Nelson, and L. Hernquist, *Lens galaxies in the Illustris simulation: power-law models and the bias of the Hubble constant from time-delays*, [arXiv:1507.0793](#).
- [11] C. R. Keeton and L. A. Moustakas, *A New Channel for Detecting Dark Matter Substructure in Galaxies: Gravitational Lens Time Delays*, *Astrophys. J.* **699** (2009) 1720–1731, [[arXiv:0805.0309](#)].
- [12] M. Oguri and P. J. Marshall, *Gravitationally lensed quasars and supernovae in future wide-field optical imaging surveys*, *Mon.Not.Roy.Astron.Soc.* **405** (2010) 2579–2593, [[arXiv:1001.2037](#)].
- [13] **LSST Science, LSST Project** Collaboration, P. A. Abell et al., *LSST Science Book, Version 2.0*, [arXiv:0912.0201](#).
- [14] **LSST** Collaboration, Z. Ivezić, J. A. Tyson, R. Allsman, J. Andrew, and R. Angel, *LSST: from Science Drivers to Reference Design and Anticipated Data Products*, [arXiv:0805.2366](#).
- [15] K. Liao, T. Treu, P. Marshall, C. D. Fassnacht, N. Rumbaugh, et al., *Strong Lens Time Delay Challenge: II. Results of TDC1*, *Astrophys.J.* **800** (2015), no. 1 11, [[arXiv:1409.1254](#)].
- [16] S. Miyazaki, Y. Komiyama, H. Nakaya, Y. Kamata, Y. Doi, T. Hamana, H. Karoji, H. Furusawa, S. Kawanomoto, T. Morokuma, Y. Ishizuka, K. Nariai, Y. Tanaka, F. Uruguchi, Y. Utsumi, Y. Obuchi, Y. Okura, M. Oguri, T. Takata, D. Tomono, T. Kurakami, K. Namikawa, T. Usuda, H. Yamanoi, T. Terai, H. Uekiyo, Y. Yamada, M. Koike, H. Aihara, Y. Fujimori, S. Mineo, H. Miyatake, N. Yasuda, J. Nishizawa, T. Saito, M. Tanaka, T. Uchida, N. Katayama, S.-Y. Wang, H.-Y. Chen, R. Lupton, C. Loomis, S. Bickerton, P. Price, J. Gunn, H. Suzuki, Y. Miyazaki, M. Muramatsu, K. Yamamoto, M. Endo, Y. Ezaki, N. Itoh, Y. Miwa, H. Yokota, T. Matsuda, R. Ebinuma, and K. Takeshi, *Hyper Suprime-Cam*, .
- [17] E. V. Linder, *Exploring the expansion history of the universe*, *Phys.Rev.Lett.* **90** (2003) 091301, [[astro-ph/0208512](#)].
- [18] **Planck** Collaboration, P. Ade et al., *Planck 2015 results. XIII. Cosmological parameters*, [arXiv:1502.0158](#).
- [19] **Planck** Collaboration, P. Ade et al., *Planck 2015 results. XIV. Dark energy and modified gravity*, [arXiv:1502.0159](#).
- [20] **BOSS** Collaboration, L. Anderson et al., *The clustering of galaxies in the SDSS-III Baryon Oscillation Spectroscopic Survey: baryon acoustic oscillations in the Data Releases 10 and 11 Galaxy samples*, *Mon.Not.Roy.Astron.Soc.* **441** (2014), no. 1 24–62, [[arXiv:1312.4877](#)].
- [21] A. G. Sanchez, E. A. Kazin, F. Beutler, C.-H. Chuang, A. J. Cuesta, et al., *The clustering of galaxies in the SDSS-III Baryon Oscillation Spectroscopic Survey: cosmological constraints from the full shape of the clustering wedges*, *Mon.Not.Roy.Astron.Soc.* **433** (2013) 1202–1222, [[arXiv:1303.4396](#)].
- [22] **SDSS** Collaboration, M. Betoule et al., *Improved cosmological constraints from a joint analysis of the SDSS-II and SNLS supernova samples*, *Astron.Astrophys.* **568** (2014) A22, [[arXiv:1401.4064](#)].
- [23] B. Audren, J. Lesgourgues, K. Benabed, and S. Prunet, *Conservative Constraints on Early Cosmology: an illustration of the Monte Python cosmological parameter inference code*, *JCAP* **1302** (2013) 001, [[arXiv:1210.7183](#)].
- [24] L. Knox, *On precision measurement of the mean curvature*, *Phys.Rev.* **D73** (2006) 023503, [[astro-ph/0503405](#)].

- [25] H. Zhan, L. Knox, and J. A. Tyson, *Distance, Growth Factor, and Dark Energy Constraints from Photometric Baryon Acoustic Oscillation and Weak Lensing Measurements*, *Astrophys. J.* **690** (2009) 923–936, [[arXiv:0806.0937](#)].
- [26] **LSST Dark Energy Science** Collaboration, A. Abate et al., *Large Synoptic Survey Telescope: Dark Energy Science Collaboration*, [arXiv:1211.0310](#).
- [27] D. Huterer and M. S. Turner, *Constraining the properties of dark energy*, [astro-ph/0103175](#). [AIP Conf. Proc.586,297(2001)].
- [28] A. Albrecht et al., *Findings of the Joint Dark Energy Mission Figure of Merit Science Working Group*, [arXiv:0901.0721](#).
- [29] G. Efstathiou and J. R. Bond, *Cosmic confusion: Degeneracies among cosmological parameters derived from measurements of microwave background anisotropies*, *Mon. Not. Roy. Astron. Soc.* **304** (1999) 75–97, [[astro-ph/9807103](#)].

A Lensing constraints on H_0

A.1 H_0 in ow CDM and ow_z CDM models

We show the constraints on H_0 from D_A and $D_{\Delta t}$ combined with the Planck distance prior.

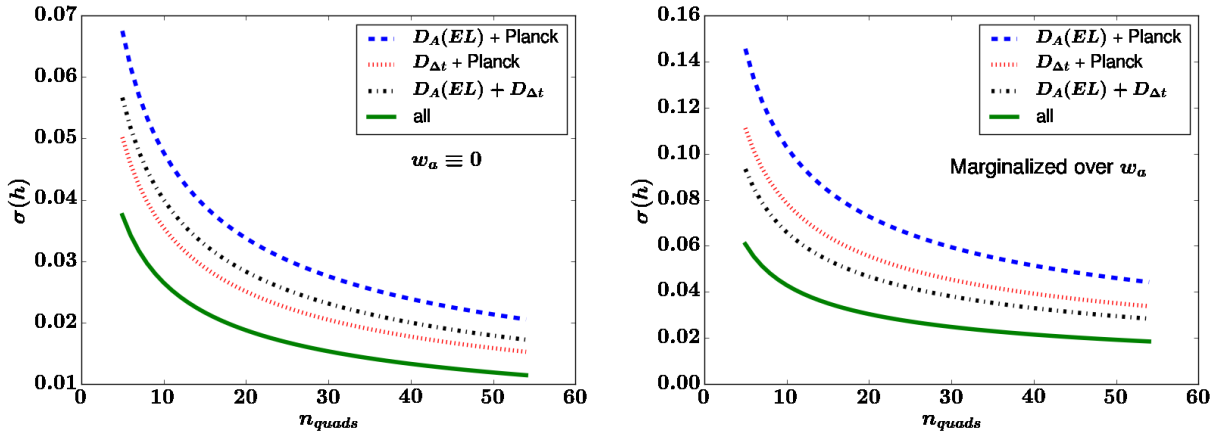


Figure 9: The 1- σ uncertainty in $h = H_0/100$ km/s/Mpc from time-delay lenses as a function of the number of quadruply imaged lenses for the (left) ow CDM model, and (right) ow_z CDM model.

Figure 9 shows the expected 1- σ uncertainties in h from strong lenses combined with the Planck distance priors. As $D_{\Delta t}$ is mostly sensitive to H_0 , the constraining power of $D_{\Delta t} + \text{Planck}$ (red dotted line) is more powerful than that of $D_A + \text{Planck}$ (blue dashed line). When w is fixed as a constant (ow CDM model, left panel), $D_{\Delta t} + \text{Planck}$ are more powerful than $D_{\Delta t} + D_A$ (black dot-dashed line). When w is allowed to vary (ow_z CDM model, right panel), however, $D_{\Delta t} + D_A$ is more powerful than $D_{\Delta t} + \text{Planck}$. This is due to the degeneracies between H_0 , Ω_k and w from the linear CMB constraints alone [29], which cannot be broken by $D_{\Delta t}$. However, ref. [3] has shown that the main degeneracy from CMB constraints is between w and H_0 , and as shown in section 3.1, the combination of lensing distances is powerful in breaking the degeneracy between Ω_k and w . Thus, the combination of Planck and the lensing distances shows 30% improvement in constraining h .

A.2 H_0 in flat Λ CDM model

We show the constraints on H_0 for the Λ CDM model in figure 10.

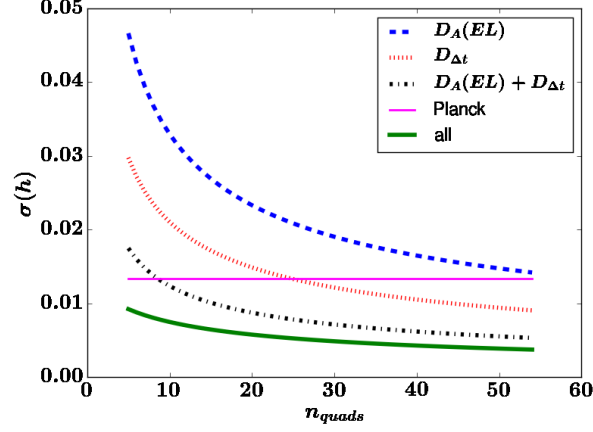


Figure 10: Same as figure 9, but for the flat Λ CDM model. Here the blue dashed, red dotted and black dash-dot lines are from the lensing distances alone, not combined with Planck. We show the constraints from Planck as the horizontal magenta solid line and Planck + lensing distances as the green solid line. Planck-precision constraint in h is achievable with 10 lenses when we use both D_A and $D_{\Delta t}$, while we need 25 lenses to achieve the same constraint from $D_{\Delta t}$ alone.

Assuming that 5% precision measurements in individual distance (both D_A and $D_{\Delta t}$) are achievable from lens systems, 10 lenses are enough to measure the Hubble constant to the same precision as Planck. The number of required lenses to achieve the same precision increases to 25 if constraints are from $D_{\Delta t}$ only.

B Constraints assuming the flat universe

In section 3.1, we have shown that the lensing distances are powerful probes for the curvature of the universe. Specifically, D_A and $D_{\Delta t}$ respond to curvature differently in w_0 - w_a plane, thus the combination of two gives a strong constraint on Ω_k . We repeat the same analysis for the flat universe model ($\Omega_k \equiv 0$). The model parameters are summarized as

$$\vec{\theta} \in \{\Omega_m, w, h\} \quad (\text{flat } w\text{CDM model}), \quad (\text{B.1})$$

and

$$\vec{\theta} \in \{\Omega_m, w_0, w_a, h\} \quad (\text{flat } w_z\text{CDM model}). \quad (\text{B.2})$$

The constraining contours for these models are shown in figures 11 and 12.

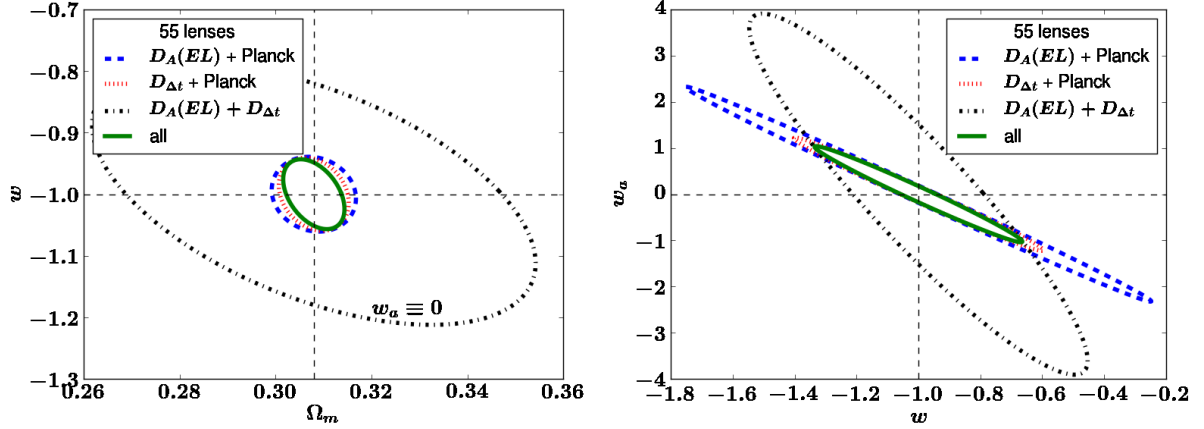


Figure 11: Same as figure 5, but for the flat (left) w CDM and (right) w_z CDM model.

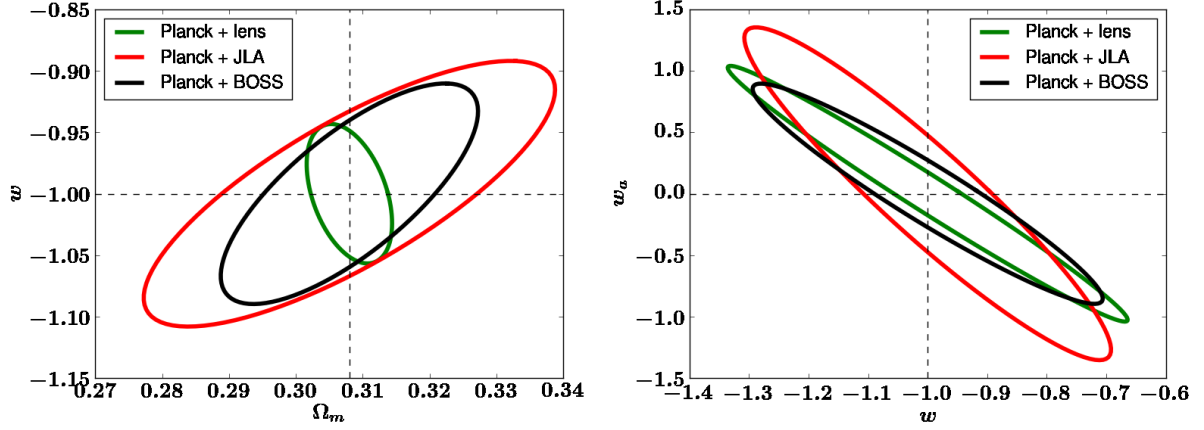


Figure 12: Same as figure 6, but for the flat (left) w CDM and (right) w_z CDM model.

Figure 11 shows that under the flatness assumption, the constraints from $D_{\Delta t} + \text{Planck}$ are already as tight as those from $D_A + D_{\Delta t} + \text{Planck}$, i.e., the constraining power from D_A in flat universe is minor. Figure 12 shows that the 55 lenses combined with Planck still constrain the equation of state better as compared to Planck + JLA and Planck + BOSS for the flat w CDM model (left panel), and comparably well as Planck + BOSS for the flat w_z CDM model (right panel).